Journal of Hazardous Materials 181 (2010) 255–262

Contents lists available at ScienceDirect

Journal of Hazardous Materials

journal homepage: www.elsevier.com/locate/jhazmat

Radiological and instrumental neutron activation analysis determined characteristics of size-fractionated fly ash

T.K. Peppas, K.L. Karfopoulos, D.J. Karangelos, P.K. Rouni, M.J. Anagnostakis*, S.E. Simopoulos

Nuclear Engineering Department, School of Mechanical Engineering, National Technical University of Athens, 15780 Athens, Greece

ARTICLE INFO

Article history:
Received 3 December 2009
Received in revised form 27 April 2010
Accepted 2 May 2010
Available online 7 May 2010

Keywords:
Fly ash
Radioactivity
Radon exhalation
INAA

ABSTRACT

The concentration of trace elements and radionuclides in fly ash particles of different size can exhibit significant variation, due to the various processes taking place during combustion inside a coal-fired power plant. An investigation of this effect has been performed by analyzing samples of fly ash originating in two different coal-fired power plants, after separation into size fractions by sieving. The samples were analyzed by gamma-ray spectrometry, including low-energy techniques, radon exhalation measurement and instrumental neutron activation analysis for the determination of Al, As, Ga, K, La, Na, Mn, Mg, Sr, Sc, and V. Variations are observed in the results of various samples analyzed, while the activity balances calculated from the results of individual size fractions are consistent with those of the raw ash samples. Correlations among the radionuclides examined are also observed, while individual nuclide behavior varies between the two types of fly ash examined.

1. Introduction

It is well known that the concentration of trace elements and radionuclides in fly ash exhibits significant variation among different size fractions [1]. Research performed at the Nuclear Engineering Department of the National Technical University of Athens (NED-NTUA) has shown that the radiological characteristics of fly ash collected at different sampling points in a coal-fired power plant can exhibit significant variations, particularly with respect to the concentration of uranium series radionuclides ^{238}U and ^{210}Pb [2] presumably due to the fly ash size fractionation. Furthermore, differences in the properties of fly ash size fractions may be of interest for the utilization of fly ash [3]. In the present work, an investigation of such phenomena is attempted by the radiological analysis of size-fractionated fly ash samples.

The aim of the work was to demonstrate and identify differences in the radiological characteristics of the various size fractions of fly ash, with a view to utilizing such observations to better understand variations among ash sampling points already observed in the previous investigations. Since an exhaustive investigation of the complex phenomena involved would require extensive and costly sampling and analysis, the scope of the present research is limited to the analysis of two contrasting fly ash samples, in order to refine analysis techniques and identify areas of interest for further study.

2. Background

Inorganic elements that are naturally present in the coal are usually enriched in the fly ash produced by coal-fired power plants, due to the removal of organic material and water during combustion. The various chemical elements exhibit different behavior during this process, due to the differences in their physicochemical properties as well as their mineralogical form. Many volatile elements are subject to an evaporation–condensation mechanism, leading to preferential enrichment on the finer fly ash particles, due to their increased surface area [1].

The natural radionuclides that are present in the coal will also take part in these processes, leading to the production of ashes with activity concentration higher than that of the feed coal, characterized as a Technologically Enhanced Naturally Occurring Radioactive Material (TENORM).

Variations of activity concentration with particle size have already been observed in fly ash, although behavior patterns are difficult to identify due to the many parameters involved [4]. In many cases, uranium and lead isotopes have been found to be preferentially enriched in finer fly ash particles, while radium and thorium isotopes display weaker trends [5,6]. Similar conclusions have been drawn from the analysis of Greek fly ash, originating in the Ptolemais lignite-burning power plants [7].

* Corresponding author. Tel.: +30 210 7722912; fax: +30 210 7722914.
E-mail address: managno@nuclear.ntua.gr (M.J. Anagnostakis).

0304-3894/$ – see front matter © 2010 Elsevier B.V. All rights reserved.
doi:10.1016/j.jhazmat.2010.05.005

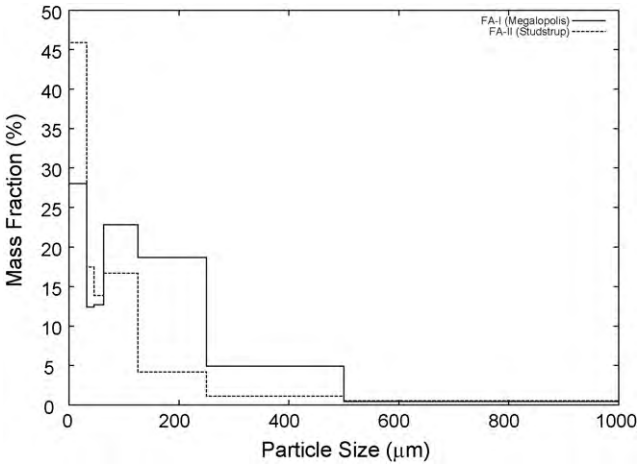

Fig. 1. Particle size distributions of the samples analyzed (weight basis).

3. Sample preparation

Two different types of fly ash were analyzed in the present work:

- Fly ash I (FA-I) has been collected at the Megalopolis B power plant, located in Megalopolis, Greece. This power plant is fed with locally mined lignite, of low calorific value, high moisture and high ash content, characterized by high (~6%) sulfur content [8]. The fly ash produced, belonging to class W according to EN197-1, has been the subject of several radiological investigations [2,9,10].
- Fly ash II (FA-II) has been collected at Studstrup Power Station unit 4 (SSV4), in Studstrup, Denmark. The power station is a 350 MWe pulverized coal-fired unit commissioned in 1985, with a once-through single reheat type boiler fitted with 24 low NO_x burners, four of which have been converted for biomass co-firing [11].

The fuel mixture consists of imported South African and Colombian coal, mixed with varying amounts of locally obtained biomass. Straw was used during the sampling period, at an energy share of 5%. This sample was collected in the framework of UCOR project, which examined the utilization of residues from biomass co-combustion in pulverized coal boilers. Chemical analyses performed by UCOR participants have identified the ash produced at SSV4 as belonging to class V according to EN197-1, with a high K_2O and P_2O_5 content due to the presence of biomass in the feed mixture [12].

Samples of both types of fly ash were collected from ash storage lots and cannot be considered as representative of any specific point in the flue gas pathway. The analysis results should therefore be interpreted as giving an overall qualitative picture of the situation in the respective power plants.

Each type of fly ash was separated into seven size fractions by sieving with a RETSCH AS-200 sieve shaker, equipped with wire mesh sieves with apertures of 32 μm, 45 μm, 63 μm, 125 μm, 250 μm and 500 μm. Sieving was performed at an amplitude of 2 mm, continuing until the weight of each fraction changed by less than 1% in a 2-min interval. The particle size distributions determined in this manner are presented in Fig. 1 on a weight basis.

After collecting the size fractions, radon exhalation measurements were performed on the FA-I fractions, as described in Section 4.2. FA-II fractions were not analyzed for radon exhalation due to their lower ^{226}Ra content. Subsequently, all fractions were packaged in standardized cylindrical plastic containers for gamma-spectrometric measurement. Two different container sizes were used, with volumes of 282 mL and 80 mL, depending on the amount of sample available.

The containers were sealed with an epoxy resin against the escape of radon and set aside for a period of 24 days, to allow for establishment of equilibrium between ^{226}Ra and its short-lived decay products ^{222}Rn, ^{218}Po, ^{214}Pb and ^{214}Bi. For each of FA-I and FA-II, one extra container was filled with the original, unfractionated fly ash.

Aliquots of the FA-I fractions, other than those used for gamma-ray spectrometry, were also used for instrumental neutron activation analysis (INAA), as described in Section 4.3.

4. Analytical methods

4.1. Gamma-ray spectrometry

All samples were analyzed on a closed-end coaxial Extended Range (XtRa) germanium detector, with a relative efficiency of 104.5%, housed in a shield of old steel and equipped with standard signal processing electronics. The detector, shielding and all electronic modules have been manufactured by Canberra. The detector system has been calibrated using a QCY.48 mixed nuclide solution certified by Amersham, for a range of standardized sample-detector geometries. Further details concerning the gamma-ray spectrometry method used have been given elsewhere [13].

It should be noted that, for the FA-I size fraction larger than 500 μm the amount collected was not enough to fill even the smallest standardized container available. In order to analyze this fraction, approximate calibration coefficients were determined by Monte-Carlo methods, transferring the efficiencies of the closest available calibrated geometry. Calculations were performed using the computer codes PENELOPE [14] and ETNA [15]. Furthermore, the density of the same size fraction in FA-II was found to be at the lower end of the range where the self-absorption correction correlations used at NED-NTUA are applicable. For these reasons, all activity concentration results for the >500 μm fractions should be considered approximate and are not included in the figures presented.

Spectrum collection times ranged from 70 ks to 320 ks and were adequate for the achievement of satisfactory uncertainty on the XtRa detector for all nuclides analyzed. All spectrum analysis was performed using the SPUNAL computer code, which has been developed in-house at NED-NTUA for the analysis of gamma spectra in a Unix environment. The following nuclides were determined:

- ^{210}Pb, employing the photons at 46.52 keV;
- ^{238}U, via its daughter ^{234}Th in equilibrium, which emits photons at 63.29 keV;
- ^{226}Ra, via its daughter nuclides ^{214}Pb and ^{214}Bi, after obtaining secular equilibrium as described in Section 3. Photons at 295.22 keV, 351.99 keV (^{214}Pb) and 609.32 keV, 1120.28 keV and 1764.51 keV (^{214}Bi) were used. In one case (FA-I, >500 μm), where radon-tight sealing was not possible due to the small amount of sample available, ^{226}Ra activity was calculated from the multiplet peak at 186 keV. The contribution of ^{235}U to the multiplet was estimated from the activity of ^{238}U, assuming a natural isotopic composition for uranium;
- ^{232}Th via its decay products ^{228}Ac (338.40 keV, 911.07 keV), ^{212}Pb (238.63 keV) and ^{208}Tl (583.14 keV). It should be noted that, due the long half-lives of the nuclides involved, equilibrium for the thorium series cannot strictly be ensured in reasonable time after sampling. However, as ^{228}Ac, ^{212}Pb and ^{208}Tl activities were found to be statistically equal in almost all samples analyzed, radioactive equilibrium was assumed for the entire thorium series and the mean value calculated as ^{232}Th for each sample;

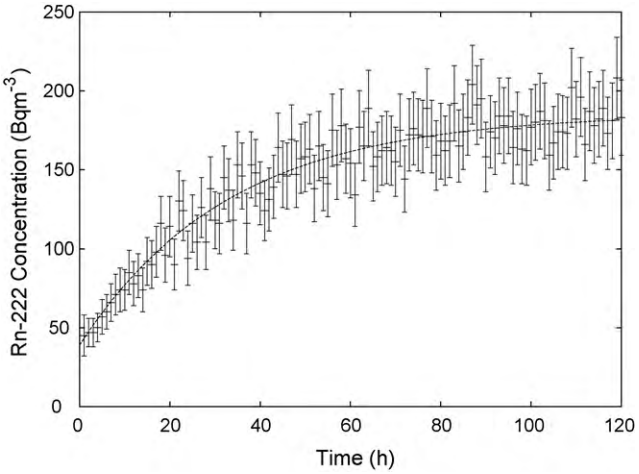

Fig. 2. Radon exhalation measurement data.

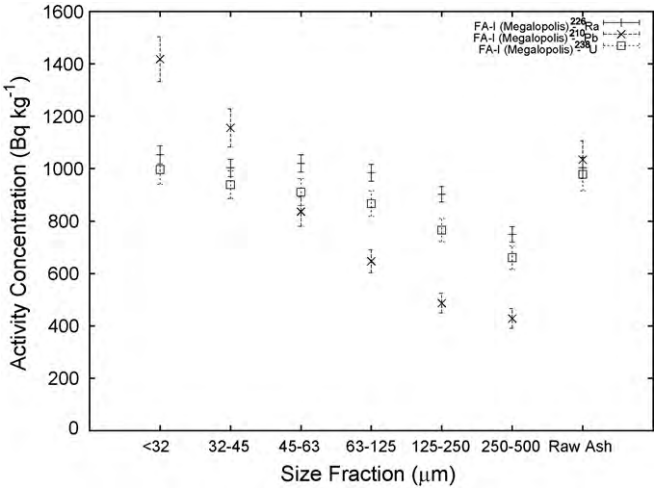

Fig. 3. Gamma-ray spectrometry analysis results: FA-I (Megalopolis), uranium series nuclides.

- ^{40}K, via its photons at 1460.71 keV. The efficiency for this particular peak was determined using a source of pure KCl, providing a better estimate than the interpolation performed by the calibration curve.

For the analysis of ^{210}Pb and ^{234}Th photons, at 46.52 keV and 63.29 keV respectively, an efficiency correction factor, calculated using an experimental–numerical method, was used to account for self-absorption due to the low energy of the photons involved [13,16].

4.2. Radon exhalation measurement

The ^{222}Rn exhalation rate of the FA-I fractions was determined using a closed-can method. The samples were enclosed in a 6 L steel vessel. An AlphaGUARD PQ2000Pro active radon monitor was externally attached to the vessel, along with a timer-controlled, gas-tight air pump, using flexible Tygon tubing. A glass fiber radon decay product filter, provided by the instrument manufacturer to prevent unnecessary contamination of the ionization chamber, was connected in-line between the sample vessel and instrument chamber. Radon concentration inside the vessel was followed for a duration of not less than 120 h. Particularly for the >500 μm fraction, due to the small amount of sample available, a smaller (500 mL) glass vessel, equipped with a Teflon valve mounted on a ground-glass joint was used instead of the steel vessel.

A typical radon exhalation measurement curve, generated from the analysis of the finest (<32 μm) fraction of FA-I, is presented in Fig. 2. The radon exhalation rate E can be determined by fitting the experimental concentration data $C(t)$ to an exponential curve of the form:

$$C(t) = C_0 exp(-\lambda t) + \frac{E}{\lambda V}(1 - \exp(-\lambda t)) \quad (1)$$

In this equation, V is the total air volume in the system and λ is an effective decay constant, accounting for both radioactive decay of radon and leakage losses. For all measurements, the sample volume was smaller than 1/10th of the free chamber volume; it can therefore be assumed that the steady-state exhalation rate does not differ significantly from the free exhalation rate [17].

In most materials, only a small fraction of the radon produced by radium decay is released from the material grains and exhaled to the surrounding atmosphere. The fraction of the produced radon that is released from the material grains to the pore space air has been variously termed as the emanation factor, emanation coefficient, emanation fraction or emanation power. By applying simple diffusion models found in the literature [18], it can be easily seen that, if the sample is thin compared to the bulk diffusion length for radon, the emanation coefficient f can be simply evaluated as:

$$f = \frac{\varepsilon}{\lambda(^{222}\mathrm{Rn})R} \quad (2)$$

where ε is the exhalation rate of ^{222}Rn per unit mass and R is the activity concentration of ^{226}Ra.

Experimental measurement has shown that the emanation coefficient of fly ash is low, with typical values in the range of 1–5% [19], presumably due to the particle formation processes following combustion.

4.3. Instrumental neutron activation analysis

Instrumental neutron activation analysis (INAA) for the determination of Al, As, Ga, K, La, Na, Mn, Mg, Sr, Sc, and V was performed using a 10 Ci ^{241} Am–Be source, housed in a 1 m^3 water tank, and an XtRa Ge detector (relative efficiency 104.5%) for the gamma spectroscopic analysis of the activated samples. A 24 mL aliquot of each size fraction of FA-I was placed in a watertight polyethylene holder and irradiated according to two scenarios:

- Scenario A for the determination of the short-lived radionuclides Al, Mg and V: 1 h of irradiation followed by a 15 min gamma-ray spectroscopic analysis, with a 50 s delay between irradiation and analysis.
- Scenario B for the determination of the radionuclides As, Ga, K, La, Mn, Na, Sr and Sc with longer half-lives: 110 h of irradiation followed by gamma-spectroscopic analysis after a 4 min delay. Three different spectra were collected for each sample, with durations of 1 h, 3 h and 13 h respectively, to better determine activation products with different half-lives.

The total analysis procedure for all the elements that were determined has been calibrated using NIST Standard Reference Material 1633b (Coal Fly Ash).

5. Analysis results

5.1. Gamma-ray spectrometry

Gamma-spectroscopic analysis results for all samples, determined as described in Section 4.1 are presented in Figs. 3–6. The

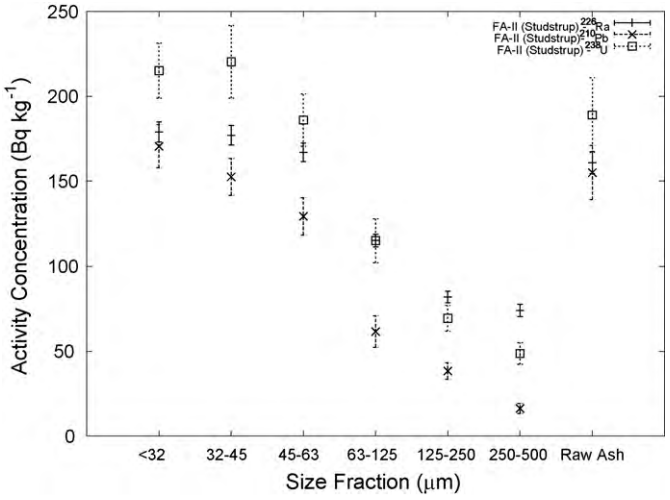

Fig. 4. Gamma-ray spectrometry analysis results: FA-II (Studstrup), uranium series nuclides.

data points are accompanied by error bars representing the combined standard uncertainty, as estimated from both the counting uncertainty and the following systematic components:

- efficiency calibration source uncertainty,
- efficiency calibration curve fitting uncertainty, and
- self-absorption correction uncertainty, where applicable.

It should be noted that, for the FA-II fraction larger than 500 μm, the thorium series was found to be in disequilibrium, with ^{228}Ac activity equal to approximately twice that of the ^{220}Rn decay products, ^{212}Pb and ^{208}Tl. However, this fraction has been eliminated from the discussion due to the concerns mentioned in Section 4.1.

It can be seen that FA-I and FA-II have different radiological characteristics, with FA-I containing significantly higher amounts of uranium series nuclides. Thorium-232 and ^{40}K are at comparable levels in both types of fly ash, with FA-II exhibiting higher activities in some size fractions.

Variations in the activity concentrations can be clearly seen, in most cases strongly correlated to the particle size. Uranium series nuclides ^{226}Ra, ^{238}U and ^{210}Pb are preferentially enriched in the finer particles in both samples, while ^{232}Th is increased in the finer fractions of FA-II but not FA-I. The activity concentration

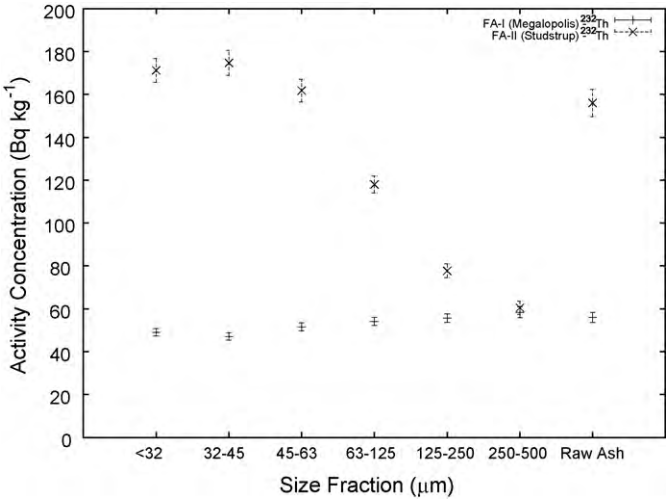

Fig. 5. Gamma-ray spectrometry analysis results: ^{232}Th.

of ^{40}K in FA-I exhibits some increase towards the coarser end of the size range, while a much more pronounced increase is seen in FA-II.

5.2. Radon exhalation

Radon-222 exhalation rates per unit mass for all FA-I fractions are presented in Table 1, accompanied by combined standard uncertainties estimated from curve fitting, chamber volume and instrument calibration uncertainty components. The table also includes emanation coefficients for all samples, although the values for the >500 μm fraction have been obtained using approximate results of ^{226}Ra activity concentration, as described in Section 4.1. No attempt was made to measure radon exhalation rates from FA-II fractions, as the activity concentration of ^{226}Ra was found to be much lower than that in FA-I.

It can be seen that the exhalation rates are rather low, well within the range of values reported in the literature for fly ash. The emanation coefficient does not exceed 2.4%, also comparable to values reported by other researchers [2,19,20].

It is obvious that there exists variability among size fractions in the analysis results. It seems that the exhalation rate exhibits a minimum at the middle of the size range, increasing towards both smaller and larger grain sizes. However, due to the rather low exhalation rates, measurement uncertainties are significant and do not permit a clear identification of trends.

It can be argued that two opposing phenomena are at work: as grain sizes decrease, specific surface area increases, leading to increased radon emanation. On the other hand, it is obvious by visual examination that the largest size fractions contain increasing amounts of partially burnt lignite present as carbon char. It is plausible to assume that the behavior of radon gas in such particles

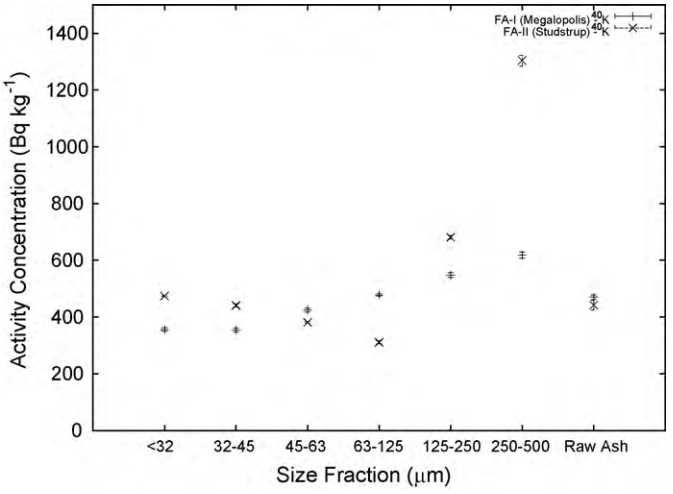

Fig. 6. Gamma-ray spectrometry analysis results: ^{40}K.

Table 1
Radon exhalation measurement results.

Size fraction (μm)	Exhalation rate (μBq kg^{-1} s^{-1}, ±1σ)	Emanation coefficient (%, ±1σ)
<32	36 ± 2.0	1.7 ± 0.13
32–45	33 ± 1.9	1.6 ± 0.13
45–63	27 ± 1.5	1.2 ± 0.10
63–125	26 ± 1.5	1.3 ± 0.10
125–250	32 ± 1.9	1.7 ± 0.14
250–500	38 ± 2.4	2.4 ± 0.17
>500	30 ± 2.2	2.4 ± 0.24
Raw ash	37 ± 2.1	1.8 ± 0.12

is nearer to that of lignite, which is known to exhibit much higher exhalation rates [2], than to that of glassy fly ash particles.

This hypothesis is supported by the fact that the emanation coefficient exhibits an increasing trend towards the coarse end of the size range, in contrast to what would be expected if particle size was the only determining factor.

5.3. Instrumental neutron activation analysis

The results of the instrumental neutron activation analyses of FA-I fractions are presented in Table 2, accompanied by combined standard uncertainties calculated from the following components:

- sample spectrum counting uncertainty,
- calibration spectrum counting uncertainty, and
- reference material uncertainty, as reported on the SRM certificate.

The concentrations determined are generally in agreement with values reported by other researchers for Megalopolis fly ash [9,21]. Elements Al, As, K, Mg and Mn display variation among the size fractions. Some variation can also be seen for other elements, but increased uncertainties do not permit clear identification of trends.

6. Discussion

6.1. Radioactivity balance

The particle size distribution of the fly ash samples analyzed, presented in Section 3, can be used in conjunction with the radionuclide activity concentrations presented in Section 5 to determine the corresponding activity concentrations for the raw fly ash. These values have been calculated and can be seen in Table 3, in comparison to the specific activities determined by direct gamma-spectroscopic analysis of an aliquot of the whole ash, before fractionation.

It has already been noted that some approximations have been employed in the determination of activity concentration values for the fraction with grain size larger than 500 μm. As the weight contribution of this fraction is less than 5% in both samples, it is believed that these approximations should not have any significant effect on the calculation results.

The two sets of activity concentration values are in good agreement, with discrepancies of the same order of magnitude as the measurement uncertainties. To further examine the statistical significance of these discrepancies, z-scores were calculated according to the formula:

$$z = \frac{R_f - R_w}{\sqrt{(s_f)^2 + (s_w)^2}} \quad (3)$$

In this formula, R_f is the activity concentration calculated from the size fraction results, s_f is the corresponding combined standard uncertainty and R_w and s_w are the same quantities for the whole ash analysis. As can be seen in Table 3, no statistically significant discrepancy is detected by this test, as in all cases $|z| < 1.96$, except for that of ^{40}K in FA-I. It should however be noted that $z > 0$ for every nuclide and in both samples, which should be taken as an indication that some systematic effect is present. In fact, it can be argued that the z-scores calculated using the combined standard uncertainty are overly conservative, as this uncertainty contains calibration source and fitting components which are correlated among samples, as all analyses were performed with the same detector set-up.

It is interesting to note that the greatest deviation is observed for ^{210}Pb, as it has already been shown that this nuclide dis-

Table 2
Instrumental neutron activation analysis results (FA-I).

Element	Concentration (ppm, ±1 σ)						
	<32 μm	32–45 μm	45–63 μm	63–125 μm	125–250 μm	250–500 μm	Raw ash
Al	70,844 ± 2,371	69,715 ± 2,333	80,291 ± 2,647	89,585 ± 2,822	89,743 ± 2,914	98,092 ± 3,234	76,536 ± 2,411
As	42 ± 5	25 ± 5	11 ± 4	6 ± 4	6 ± 5	–	18 ± 4
Ga	19 ± 5	15 ± 6	11 ± 5	15 ± 5	12 ± 6	–	15 ± 4
K	11,150 ± 1,051	11,526 ± 985	13,319 ± 1,067	14,981 ± 1,122	16,094 ± 1,205	18,226 ± 1,301	13,245 ± 1,015
La	48 ± 6	55 ± 6	55 ± 6	56 ± 6	58 ± 6	54 ± 6	54 ± 5
Mg	2,236 ± 318	2,489 ± 293	3,165 ± 355	2,985 ± 342	3,221 ± 380	3,318 ± 398	2,580 ± 337
Mn	611 ± 17	591 ± 16	523 ± 15	470 ± 13	444 ± 12	427 ± 12	509 ± 14
Na	3,350 ± 67	3,368 ± 67	3,391 ± 68	3,415 ± 70	3,370 ± 68	3,361 ± 68	3,270 ± 67
Sc	11 ± 7	19 ± 7	19 ± 7	22 ± 7	20 ± 8	22 ± 8	19 ± 7
Sr	2,367 ± 665	2,168 ± 651	1,935 ± 607	1,894 ± 600	1,126 ± 487	1,117 ± 496	1,820 ± 567
V	299 ± 112	264 ± 110	326 ± 122	298 ± 122	254 ± 113	243 ± 116	298 ± 113

Table 3
Comparison of size fraction activity concentration weighted means with raw ash analysis results (FA-I and II).

	Activity concentration (Bq kg^{-1}, ±1σ)		Relative difference (%)	z-Score
	Raw ash analysis	Size fraction weighted mean		
FA-I				
^{226}Ra	1004 ± 40	982 ± 14	2.2	0.51
^{232}Th	56 ± 2.3	52.0 ± 0.83	7.7	1.58
^{40}K	470 ± 7.0	440 ± 8.4	6.9	2.74
^{210}Pb	1035 ± 72	908 ± 29	14.0	1.63
^{238}U	979 ± 63	887 ± 23	10.4	1.37
FA-II				
^{226}Ra	161 ± 6.4	160 ± 3.1	0.6	0.04
^{232}Th	156 ± 6.3	155 ± 3.0	0.6	0.11
^{40}K	442 ± 7.0	443 ± 2.8	0.2	0.13
^{210}Pb	155 ± 16	135 ± 6.5	14.8	1.13
^{238}U	189 ± 22	186 ± 8.9	1.6	0.13

Table 4
Correlation coefficients for each pair of radionuclides determined.

	FA-I				FA-II			
	^{232}Th	^{210}Pb	^{238}U	^{40}K	^{232}Th	^{210}Pb	^{238}U	^{40}K
^{226}Ra	−0.844	0.776	0.970	−0.915	0.994	0.987	0.996	−0.685
^{232}Th		−0.912	−0.922	0.978		0.975	0.993	−0.755
^{210}Pb			0.901	−0.930			0.990	−0.648
^{238}U				−0.977				−0.691

plays a clearly increasing trend towards the finest particle sizes while its determination is performed using low-energy photons at 46.52 keV, which exhibit significant self-absorption. As fly ash is a free-flowing powder, the finest particles are expected to preferentially collect at the bottom of the container. It is believed therefore that the increased result of the raw ash analysis is due to the lower part of the container having a greater contribution to the total count rate of ^{210}Pb.

Further investigation of such phenomena is important for the production of high quality analytical results, particularly in the determination of low-energy emitters.

6.2. Radionuclide correlations

It is evident from Figs. 3–6 that clear correlations exist among the activity concentrations of the various radionuclides in each sample. These are further demonstrated by calculating the correlation coefficient for the activity concentrations of each pair of radionuclides in the two samples, which is presented in Table 4.

The radionuclides determined in each sample can be split into two groups of positively correlated radionuclides, with negative correlation between members of different groups. In FA-I, the first group comprises of ^{226}Ra, ^{210}Pb and ^{238}U and the second of ^{232}Th and ^{40}K, while in FA-II ^{226}Ra, ^{210}Pb, ^{238}U and ^{232}Th form a single group, each element of which is negatively correlated to ^{40}K. Radionuclides belonging in a single group must exhibit similar behavior during combustion, in a manner analogous to the classification groups proposed for stable trace elements in fly ash.

6.3. Uranium series nuclides

From the results presented in Fig. 3, it is clear that uranium series nuclides ^{238}U, ^{226}Ra and ^{210}Pb are not in radioactive equilibrium in the FA-I fractions. It appears that ^{226}Ra is slightly increased compared to ^{238}U, with both nuclides displaying a small increasing trend towards the fine end of the size range. This behavior is consistent with previous investigations by NED-NTUA at Megalopolis, while marginal disequilibrium in favor of ^{226}Ra has also been observed in lignite samples from the specific power plant [2].

Similar variations can be observed in FA-II, although overall activity concentrations are much lower. In contrast to FA-I, both ^{238}U and ^{226}Ra display appreciable variation among different size fractions, which implies that ^{238}U and ^{226}Ra in SSV4 are being volatilized during combustion.

Variations in the activity concentrations of ^{238}U and ^{226}Ra could possibly be attributed to the presence of varying amounts of unburnt carbon in the size fractions, effectively diluting the radionuclides. In order to investigate this effect, loss on ignition was determined for all size fractions up to 500 μm. For each size fraction, a 1 g aliquot of dry ash was placed in a tarred porcelain crucible and slowly heated to 750 °C in a muffle furnace, where it remained for 6 h. The crucible was subsequently allowed to cool in a desiccator and weighed again. Each determination was performed in triplicate, to obtain an estimate of the uncertainty. The resulting LOI values are presented in Table 5. It can be seen that LOI is in fact different among the fractions for both samples, but to an extent that cannot completely justify the differences observed in radionuclide activity concentrations.

Lead 210 in FA-I displays a much more pronounced trend across the size range. Compared to ^{226}Ra, it is found to be deficient in coarse particles and excessive in fine ones while analysis of the raw ash indicates that, overall, ^{226}Ra and ^{210}Pb are close to radioactive equilibrium. Analysis of lignite samples from the Megalopolis B power plant in the past has shown ^{226}Ra and ^{210}Pb to be in radioactive equilibrium [2]. The disequilibrium observed in the fly ash must therefore be attributed to redistribution of ^{210}Pb during combustion and ash formation due to volatilization/condensation phenomena.

In FA-II, ^{210}Pb is found to be consistently deficient compared to ^{226}Ra, although the finer size fractions making up the bulk of the sample are at or near radioactive equilibrium. This might be an indication that some ^{210}Pb is escaping the power plant in gaseous form, but confirming this hypothesis would require more rigorous sampling of fly ash as well as analysis of bottom ash and fuels.

6.4. Thorium-232

The activity concentration of ^{232}Th in FA-I is not found to vary significantly among size fractions. This is to be expected, as thorium is commonly found in coal in refractory forms, and is consistent with previous observations at the Megalopolis power plants where no significant variation in ^{232}Th activity concentration was found at different sampling points along the flue gas pathway.

In contrast to this behavior, the activity concentration of ^{232}Th in FA-II is found to increase significantly towards the fine end of the size range, indicating that some volatile form of thorium is present during fly ash formation. This observation may be related to the fact that co-combustion of straw introduces increased amounts of chlorine to the fuel mixture [11,22]. It is therefore possible that compounds such as $ThCl_4$ which sublimates at 820 °C and would be subject to an evaporation–condensation mechanism at boiler temperatures, are formed during combustion [4].

It should be noted that, although ^{228}Ra, determined via ^{228}Ac, and ^{228}Th, determined via ^{212}Pb, were found to be in radioactive equilibrium in all but one FA-II fractions as explained in Section 4.1, radioactive equilibrium of the entire thorium series cannot be ensured in the presence of such dynamic phenomena. Further investigation of the behavior of ^{232}Th is therefore required, ideally employing methods able to directly determine its activity concentration.

Table 5
Fly ash loss on ignition at 750 °C.

Size fraction (μm)	LOI (%)	
	FA-I	FA-II
<32	2.58 ± 0.07	2.37 ± 0.04
32–45	2.56 ± 0.03	3.79 ± 0.08
45–63	1.99 ± 0.01	7.10 ± 0.21
63–125	1.72 ± 0.06	13.10 ± 0.19
125–250	2.18 ± 0.05	13.1 ± 1.2
250–500	4.79 ± 0.29	6.25 ± 0.72

Table 6
Comparison of ^{40}K activity concentration as determined by gamma spectroscopy and neutron activation (FA-I).

Size fraction (μm)	Activity concentration (Bq kg^{-1}, ±1σ)		z-Score
	Neutron activation	Gamma spectroscopy	
<32	346 ± 33	356 ± 6	−0.31
32–45	357 ± 31	354 ± 7	0.09
45–63	413 ± 33	425 ± 7	−0.36
63–125	464 ± 35	478 ± 5	−0.40
125–250	499 ± 37	548 ± 8	−1.30
250–500	565 ± 40	618 ± 11	−1.26
Raw ash	411 ± 31	470 ± 7	−1.83

6.5. Potassium-40

The activity concentration of ^{40}K is found to increase with increasing particle size in FA-I. An abrupt increase is observed in the activity concentration of ^{40}K in the coarser size classes of FA-II. Potassium-40 is usually found to exhibit limited to no particle size dependence in fly ash, and is assumed to be a tracer for the inorganic ash matrix [5]. On the other hand, the inclusion of straw in the fuel mix at SSV4 has been known to cause a significant increase in the fly ash potassium content and affect overall potassium behavior [11]. It is therefore plausible to assume that this unexpected variation in ^{40}K activity concentration in FA-II is related to the effects of biomass co-combustion on potassium chemistry.

6.6. Stable elements

INAA results point out the differences in the behavior of the 11 elements detected. Arsenic and manganese concentrations display significant enrichment in the finer size fractions. Arsenic is a well-known example of an element subject to a volatilization–condensation mechanism during combustion [1]. The increase for manganese on the other hand is rather unexpected, as it is usually classified with the lithophile elements and does not concentrate preferentially on fine particles [1,23]. Potassium, aluminum and magnesium have the opposite behavior and present depletion in the finer size fractions. No trend is clearly apparent for the remaining elements, some of which, such as scandium and lanthanum, do not usually exhibit preferential enrichment. For others, such as Ga, an increase in concentration is to be expected in the finer size fractions according to the literature, but is probably masked by measurement uncertainty.

6.7. Comparison of instrumental neutron activation analysis and gamma-ray spectrometry results

The concentration of potassium in each size fraction has been determined by instrumental neutron activation analysis, while radioactive ^{40}K was determined by gamma-ray spectrometry. Taking into account the fact that ^{40}K, a primordial radionuclide, exhibits a constant atomic abundance in nature, it is possible to convert from the elemental potassium concentration C to the activity concentration of ^{40}K in the sample R and compare the two techniques using the following formula:

$$R = \frac{aN_A \ln 2}{m_{at} T_{1/2}} C \quad (4)$$

with the following data [24]: $N_A = 6.022 \times 10^{23}$ g mole^{-1} is the Avogadro constant; $m_{at} = 39.0983$ g mole^{-1} is the atomic mass of elemental potassium; $a = 0.0117\%$ is the atomic abundance of ^{40}K; and $T_{1/2} = 1.28 \times 10^9$ is the half-life of ^{40}K.

In Table 6, the concentration of potassium determined by INAA is compared to that calculated from the gamma-ray spectroscopy analysis results. It can be seen that the two techniques are in good agreement, with differences smaller than the combined standard uncertainty in most cases.

7. Conclusions

From the analysis results presented, clear variations can be seen in the activity concentrations of natural radionuclides detected in fly ash. These variations are well correlated with particle size, as it has also been observed in other similar studies in the literature. However, individual nuclide behavior seems to be different for the two fly ash samples studied, originating in two different coal-fired power plants operating on different types of fuel.

Uranium series nuclides present similar behavior in both FA-I and FA-II, with increasing activity concentration towards the finest size fractions, although absolute activity levels are much higher in FA-I than in FA-II. Thorium-232 displays a clear increasing trend towards the finer size fractions in FA-II, while showing much smaller variation in FA-I. An opposing trend is obvious for ^{40}K in FA-II, increasing towards the coarser size fractions, while a similar but much less pronounced trend can be seen in FA-I. Based on the findings reported in the literature concerning co-combustion at SSV4, where FA-II originates, it is believed that the behavior of ^{232}Th and ^{40}K in FA-II is strongly affected by the addition of biomass to the fuel mixture.

Some indications of discrepancy are observed between the results of size fraction analysis and those of the raw ash. It is believed that this may be an effect of vertical inhomogeneity in the raw ash samples, naturally arising due to the free-flowing nature of fly ash, which however is masked by uncertainty.

The dependence of radon exhalation on particle size was also examined, with less clear results. A plausible explanation is that two opposing effects are at work, leading to an increase in the exhalation rate towards both the coarser and the finer ends of the size range.

The concentration of stable elements determined by INAA in Megalopolis fly ash samples (FA-I) is in agreement with values reported in the literature, while some elements (Al, As, K, Mn, Mg) display significant variation among the size fractions.

Acknowledgments

The authors would like to thank Mr. I. Typos of the Institute for Technology of Solid Fuels and Applications for providing assistance with the LOI determination. Co-author T.K. Peppas would like to thank the Hellenic Army General Staff for providing educational leave, during which the present work was performed.

References

[1] L.B. Clarke, L.L. Sloss, Trace Elements – Emissions from Coal Combustion and Gasification, IEA Coal Research, London, 1992.
[2] D.J. Karangelos, N.P. Petropoulos, M.J. Anagnostakis, E.P. Hinis, S.E. Simopoulos, Radiological characteristics and investigation of the radioactive equilibrium in the ashes produced in lignite-fired power plants, J. Environ. Radioact. 77 (2004) 233–246.
[3] G.S. Itskos, S. Itskos, N. Koukouzas, The effect of particle size differentiation of lignite fly ash on cement industry applications, in: Proceedings of the 2009 World of Coal Ash Conference, Lexington, KY, USA, May 4–7, 2009, http://www.flyash.info/2009/087-itskos2009.pdf.
[4] J. Tadmor, Radioactivity from coal-fired power plants: a review, J. Environ. Radioact. 4 (1986) 177–204.
[5] D.G. Coles, R.C. Ragaini, J.M. Ondov, Behavior of natural radionuclides in western coal-fired power plants, Environ. Sci. Technol. 12 (1978) 442–445.
[6] M. Flues, I.M.C. Camargo, P.S.C. Silva, B.P. Mazzilli, Radioactivity of coal and ashes from Figueira coal power plant in Brazil, J. Radioanal. Nucl. Chem. 270 (2006) 567–602.
[7] M. Manolopoulou, C. Papastefanou, Behavior of natural radionuclides in lignites and fly ashes, J. Environ. Radioact. 16 (1992) 261–271.
[8] G. Skodras, P. Grammelis, E. Kakaras, D. Karangelos, M. Anagnostakis, E. Hinis, Quality characteristics of Greek fly ashes and potential uses, Fuel Process. Technol. 88 (2007) 77–85.

[9] H. Papaefthymiou, B.D. Symeopoulos, M. Soupioni, Neutron activation analysis and natural radioactivity measurements of lignite and ashes from Megalopolis basin, Greece, J. Radioanal. Nucl. Chem. 274 (2007) 123–130.
[10] P.K. Rouni, N.P. Petropoulos, M.J. Anagnostakis, E.P. Hinis, S.E. Simopoulos, Radioenvironmental survey of the Megalopolis lignite field basin, Sci. Total Environ. 272 (2001) 261–272.
[11] P. Overgaard, B. Sander, H. Junker, K. Friborg, O. Hede Larsen, Two years' operational experience and further development of full-scale co-firing of straw, in: Proceedings of the 2nd World Conference on Biomass for Energy Industry and Climate Protection, Rome, Italy, May 10–14, 2004.
[12] Utilization of residues from biomass co-combustion in pulverized coal boilers, Final Technical Report (NNE5/1999/366), Universität Stuttgart Institut für Verfahrenstechnik und Dampfkesselwesen (IVD), Stuttgard, 2003.
[13] M.J. Anagnostakis, S.E. Simopoulos, An experimental/numerical method for the efficiency calibration of low-energy germanium detectors, Environ. Int. 22 (1997) S93–S99.
[14] F. Salvat, J.M. Fernandez-Varea, J. Sempau, PENELOPE-2006: A Code System for Monte Carlo Simulation of Electron and Photon Transport, OECD Nuclear Energy Agency, Issy-les-Moulineaux, 2006.
[15] M.C. Lepy, M.M. Be, F. Piton, ETNA (efficiency transfer for nuclide activity measurements): software for efficiency transfer and coincidence corrections in gamma-ray spectrometry, Laboratoire National Henri Becquerel Note Technique LNHB/01/09/F, 2001.
[16] N.P. Petropoulos, M.J. Anagnostakis, S.E. Simopoulos, Photon attenuation, natural radioactivity content and radon exhalation rate of building materials, J. Environ. Radioact. 61 (2002) 257–269.
[17] C. Samuelsson, H. Pettersson, Exhalation of ^{222}Rn from porous materials, Radiat. Prot. Dosim. 7 (1984) 95–100.
[18] C. Samuelsson, The closed-can exhalation method for measuring radon, J. Res. NIST 95 (1990) 167–169.
[19] K.R. Smith, G.M. Crockett, W.B. Oatway, M.P. Harvey, J.S.S. Penfold, S.F. Mobbs, Radiological Impact on the UK Population of Industries Which Use or Produce Materials Containing Enhanced Levels of Naturally Occurring Radionuclides: NRPB-R327, National Radiological Protection Board, Oxon, 2001.
[20] E.A. Maraziotis, Effects of intraparticle porosity on the radon emanation coefficient, Environ. Sci. Technol. 30 (1996) 2441–2448.
[21] A. Georgakopoulos, A. Filippidis, A. Kassoli-Fournaraki, A. Iordanidis, J.L. Andreas, J.F. Fernández-Turiel, D. Llorens, Gimeno, Environmentally important elements in fly ashes and their leachates of the power stations of Greece, Energy Sources Part A: Recov. Utilizat. Environ. Effects 24 (2002) 83–91.
[22] B. Sander, K. Wieck-Hansen, Full-scale investigations on alkali chemistry and ash utilisation by co-firing of straw, in: Proceedings of the 14th European Biomass Conference, October 2005, Paris, 2005 (ISBN: 88-89407-07-7).
[23] M. Xu, R. Yan, C. Zheng, Y. Qiao, J. Han, Ch. Seng, Status of trace element emission in a coal combustion process: a review, Fuel Process. Technol. 85 (2003) 215–237.
[24] G. Pfennig, H. Klewe-Nebenius, W. Seelman-Eggebert, Karlsruher Nuklidkarte, Forschungszentrum Karlsruhe GmbH, Karlsruhe, 1998.